■ **Disordered Proteins**

Towards High-Throughput Modelling of Copper Reactivity Induced by Structural Disorder in Amyloid Peptides

Giovanni La Penna*[a] and Mai Suan Li[b, c]

Abstract: Transition metal ions often interact with disordered proteins. The affinity is high enough to compete with structured proteins, but the catalytic activity of the metal centre is often out of control and, therefore, potentially dangerous for cells. An example is a single copper ion interacting with the amyloid-β (Aβ) peptide and triplet dioxygen, an interaction that is fundamental in producing reactive oxygen species in neurodegeneration. High-throughput modelling of the Cu-Aβ-O_2 system was performed with the aim of providing a tool to dissect the structural features that characterise dangerous Cu-based catalysts in neurodegeneration. This study showed that the production of superoxide is a process with low-energy intermediate species, once a small population of high-energy Cu^I-Aβ complex is formed. This population is enhanced when Cu bridges two different peptides in 1:1 Cu:Aβ dimers. Despite the bias for high-energy reduced reactant species, the reduction of Cu^{II}-Aβ product by superoxide can also occur, in addition to that by ascorbate, because the structural disorder produces a small population of oxidant species characterised by unstable Cu^{II} coordination, coexisting with the most abundant reductant species, characterised by stable Cu^{II} coordination.

Introduction

For chemical purposes and inspired by enzymes, scientists have designed efficient catalysts by using structured ligands. The structure of the ligand is favourable for the catalytic purpose if it makes the catalyst robust, selective and unable to deliver the metal ions to competitors. In a cell, especially when a pathological state occurs, these conditions are not fulfilled. Metal ions are released by ligands, and interaction of other ligands with the ions leads to new and unpredictable catalytic activities. Therefore, in many biological circumstances, we observe weakly coordinated transition metal ions exhibiting efficient catalytic activity that must be understood and, possibly, silenced. Under these circumstances, it is more difficult, compared to structured ligands, to understand and eventually predict the reactivity of such complexes. One example is provided by the Cu–amyloid-β complex, which is described in the following.

The interactions between the amyloid-β (Aβ) peptide and copper produce transient catalysts that activate dioxygen and produce reactive oxygen species (ROS).[1,2] This activation has been addressed as an important pathway for triggering cell death in neurodegeneration,[3–5] and models for dioxygen activation have been proposed on the basis of calculations.[6–8] Since the affinity of Aβ for Cu is relatively high, the Aβ peptide is a candidate for sequestering Cu from other partners, which may efficiently silence its reactivity.

The intrinsic disorder of the Aβ peptide makes any mechanistic description of dioxygen activation difficult. Cu coordination to Aβ has been proposed to prevail under physiological conditions on the basis of EPR and NMR data for the oxidised form Cu^{II}-Aβ.[9,10] The reduced form, Cu^I-Aβ, has been also investigated,[11–15] but it is not stable under ambient conditions in the presence of dioxygen.[14] In the Cu^{II} complex identified as **Ia**, Cu^{2+} is bound in a square-planar geometry to N and O of Asp1, Nδ1 of His 6 and an imidazole N atom of His13 or His14, either of the same peptide or of another peptide in a multimeric state. Despite the constraints imposed by this conformation, significant distortions of this coordination modulate the interactions of Cu^{II} with both equatorial and axial ligands, and thus affect its chance of interacting with water molecules, dioxygen and further ligand groups provided by the peptide.[7,16]

The activation of dioxygen by the Cu-Aβ complex has been studied in vitro, by comparing the Cu-Aβ$_{42}$ complex with a series of reference Cu–ligand (L) complexes and the free Cu aqua ion.[17] Ascorbate, which is abundant in the central nervous system, has been used as the reducing agent to form the initial amount of reduced Cu-L (Cu^I-L) that is required to shuttle electrons towards dioxygen (see below for details). The

[a] *Dr. G. La Penna*
National Research Council (CNR)
Institute for Chemistry of Organometallic Compounds (ICCOM)
via Madonna del Piano 10, 50019 Sesto Fiorentino, Firenze (Italy)
E-mail: giovanni.lapenna@cnr.it

[b] *Prof. M. S. Li*
Polish Academy of Sciences, Institute of Physics
al. Lotników 32/46, 02-668, Warsaw (Poland)

[c] *Prof. M. S. Li*
Institute for Computational Science and Technology, SBI Building
Quang Trung Software City, Tan Chanh Hiep Ward, District 12
*Ho Chi Minh City (Vietnam)*

⬡ *The ORCID numbers for the authors of this article can be found under https://doi.org/10.1002/chem.201704654.*

These are not the final page numbers! ↗↗

steady-state production of hydroxyl radicals by Cu-Aβ_{42} was only half of that of the Cu^{II} aqua ion, which is known to not exist in cells.[18] Production of ROS by Cu-Aβ_{42} is comparable to that of Cu^{II}-(Gly-His-Lys) (Cu-GHK), a naturally occurring Cu complex involved in many biochemical pathways.[19] On the other hand, the Cu^{II}-(Asp-Ala-His-Lys) (Cu-DAHK) complex is silent in ROS production, since Cu^{II} is stable in the square-planar geometry formed by the N terminus, the His side chain and two deprotonated amide N atoms. This coordination strongly disfavours any transient Cu^{I}-DAHK formation, contrary to the case of Cu-GHK. All these complexes show, in vitro, a resting state with Cu in the oxidised form (Cu^{II}). Therefore, any tentative mechanism for catalytic ROS production involves initial coordination of Cu^{II} to the Aβ_{42} peptide. This assumption allows one to start from the information provided by the reported studies, which mostly concern the coordination of Cu^{II} to different amyloid peptides, because the coordination of Cu^{I} can be conveniently studied in vitro only in Ar atmosphere.[14]
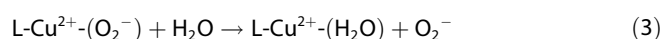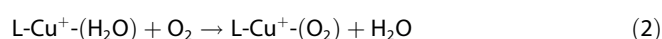
Herein, we describe a procedure to approximately rank the reactivity of Cu-Aβ as dioxygen activator, taking into account some of the architectural constraints provided by the peptide, both in monomeric and dimeric states.[20] This method is an extension of the tools described in our previous works,[16, 21] with a special emphasis on the chance for efficient electron transfer from Cu^{I} to dioxygen. In terms of number of probed structures, this work extends similar works reported in the literature tackling the same problem.[22]
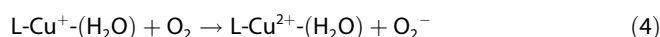
Reaction Mechanism

According to recent experimental results,[1] the first step in ROS production catalysed by Cu-Aβ is the in situ production of superoxide. The latter rapidly attacks other sites in the peptide and in its environment.[5] A possible mechanism for this first step is summarised below. The dioxygen activation is initiated by the formation of a species that can efficiently split the biradical state of dioxygen into two radicals. This species is a Cu^{I} complex that is known to be produced in a small amount by reductant molecules that are relatively abundant in cells, such as ascorbic acid [Eq. (1)]:

$$L\text{-}Cu^{2+}\text{-}(H_2O) + Asc^- \rightarrow L\text{-}Cu^+\text{-}(H_2O) + Asc^\bullet \tag{1}$$
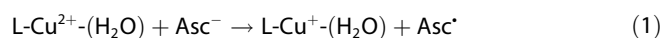
At pH 7 ascorbic acid is almost completely dissociated into ascorbate (Asc$^-$), and single-electron oxidation produces the ascorbyl radical (Asc$^\bullet$). In the framework of amyloid toxicity, L represents the Aβ peptide ligand. After the formation of an initial amount of reduced Cu^{I}-Aβ, the activation of dioxygen becomes possible in an inner-sphere reaction, provided the exchange of water molecules close to the Cu centre with dioxygen is possible [Eqs. (2), (2a) and (3)]:

$$L\text{-}Cu^+\text{-}(H_2O) + O_2 \rightarrow L\text{-}Cu^+\text{-}(O_2) + H_2O \tag{2}$$

$$L\text{-}Cu^+\text{-}(O_2) \leftrightarrow L\text{-}Cu^{2+}\text{-}(O_2^-) \tag{2a}$$

$$L\text{-}Cu^{2+}\text{-}(O_2^-) + H_2O \rightarrow L\text{-}Cu^{2+}\text{-}(H_2O) + O_2^- \tag{3}$$

Equation (2) represents the penetration of dioxygen into the inner sphere of the Cu site by replacement of water molecules eventually in contact with Cu. The energy change in this reaction depends on the extent of resonance between the triplet dioxygen state and the charge transfer from the reduced Cu centre to dioxygen with formation of a Cu^{II}-bound superoxide anion [Eq. (2a)]. Equation (3) represents the ejection of superoxide into the solvent in contact with the protein environment. This last step produces the resting state of Cu^{II}-Aβ. The above three reactions describe a hypothetical mechanism for the second step in the production of ROS by Cu-Aβ, consistent with the recent experimental results [Eq. (4)]:

$$L\text{-}Cu^+\text{-}(H_2O) + O_2 \rightarrow L\text{-}Cu^{2+}\text{-}(H_2O) + O_2^- \tag{4}$$

that is, the in situ production of superoxide by the small amount of Cu^{I}-Aβ produced by ascorbate.[1] The first step is the production of the small amount of Cu^{I}-Aβ complex [Eq. (1)].

The same mechanism is depicted in more detail in Figure 1. Reaction 4 corresponds to Equation (4), and the identity of Equation (5) holds.

$$\Delta E_4 = \Delta E_2 + \Delta E_3 \tag{5}$$

Since the turnover of Cu^{I} [Eq. (1)] must be satisfied, the ideal set of energy changes satisfying Equation (5) occurs for nega-
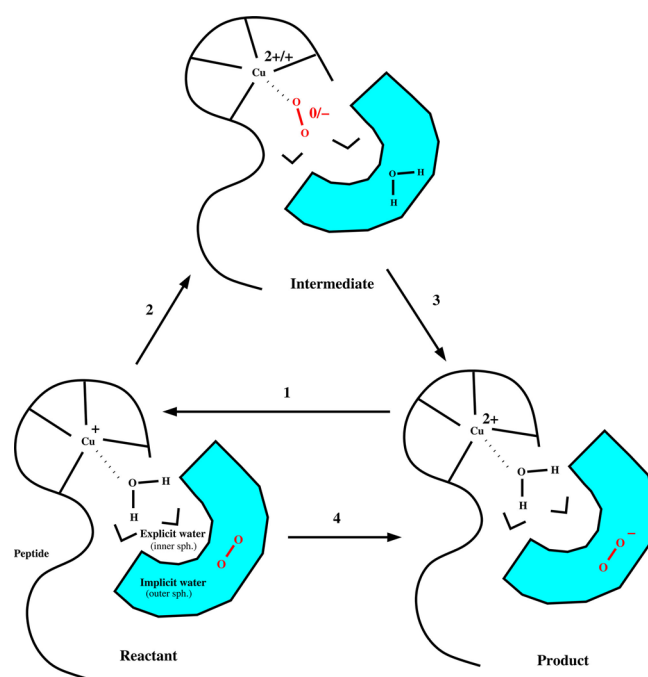

Figure 1. A possible reaction mechanism in the oxidoreductive equilibria for the production of superoxide by Cu-Aβ. Step 1 is the initiation step [Eq. (1)], that is, the initial formation of the reduced form of Cu-Aβ (Cu^{I}-Aβ); step 2 is the process of exchange of one water molecule in the vicinity of Cu^{I} with dioxygen [Eq. (2)]; step 3 is the replacement in the vicinity of Cu^{II} of the reduced dioxygen (superoxide) by a water molecule [Eq. (3)]; step 4 is the reduction of dioxygen to superoxide by the reduced form Cu^{I}-Aβ, with the formation of the resting state Cu^{II}-Aβ [Eq. (4)].

tive values of both ΔE_2 and ΔE_3, together with small absolute values of their sum ΔE_4 and small absolute values of ΔE_1. This condition makes ΔE_4 only slightly negative, as the sum of positive- and negative-energy pathways. The Cu-coordination fluxionality allows the process to be sustained with a small excess of ascorbic acid to reduce Cu^{II}-Aβ to Cu^{I}-Aβ according to Equation (1). The cycle is also partially sustained by the small amount of Cu^{II}-Aβ reduction due to superoxide when ΔE_4 is positive. The characterisation of the state denoted "Intermediate" in Figure 1 is the main goal of this work.

Below, we provide an estimate of the concentration of Cu^{I}-Aβ under the conditions used for in vitro experiments. The latter are assumed to mimic physiological conditions in the central nervous system. With C_0(CuII) and C_0(Asc) as the initial concentrations of Cu^{II}-Aβ and ascorbate, respectively, the equilibrium constant of Equation (1) is given by Equation (6):

$$K = \frac{[\text{CuI}][\text{Asc}^{\bullet}]}{[\text{CuII}][\text{Asc}^{-}]} \tag{6}$$

where CuII and CuI denote the oxidised and reduced forms, respectively, of Cu-Aβ

We define the amount of product x as the concentration of product CuI and express this quantity as the ratio of x to the initial concentration of CuII: $y = x/C_0$(CuII). Assuming x is small compared to the initial concentrations C_0 of reactants, Equation (6) becomes Equation (7):

$$K = \frac{y^2}{C_0(\text{Asc})/C_0(\text{CuII})} = \frac{y^2}{z} \tag{7}$$

where z is the ratio between initial concentrations of ascorbic acid and that of the Cu^{II}-Aβ complex. The equation can be simply written as: $\lg y = 1/2[\lg z - \Delta G_0/(RT\ln 10)]$, in which ΔG_0 is the free-energy change under standard conditions of reaction 1.

In experiments, the ratio z is usually 10, while in the central nervous system this ratio is larger. Assuming $z = 10$ and $\Delta G_0 \approx \Delta E$, in which ΔE is the energy obtained by calculations for reaction 1, we obtain a simple relation for the concentration of reduced Cu^{I}-Aβ complex with respect to the total amount of Cu-Aβ complex [Eq. (8)]:

$$\lg y = 1/2[-\Delta E/(RT\ln 10) + 1] \tag{8}$$

With these approximations, a value of 30 kJ mol^{-1} produces a concentration of Cu^{I}-Aβ of 1% of the total amount of Cu-Aβ.

The cycle from the resting state, passing through reasonable configurations for water and dioxygen in the Cu inner sphere, can be modelled at the DFT level of theory. Configurations representing the resting oxidised state are extracted from empirical models, that is, molecular dynamics (MD) simulations of Aβ(1–42) dimers including one Cu^{2+} ion per monomer, explicit water molecules and monovalent ions modelling the environment of in vitro experiments.

The transition from empirical models of Cu^{II}-Aβ to DFT models of Cu^{I}-Aβ is based on the relaxation of atoms within the DFT forces accounting for the change of oxidation state (see Methods Section). This approximation implies the assumption that all the Cu coordination geometries sampled in the reaction pathway described in Equations (1)–(3) are those of minimal reorganisation for the resting oxidised state. Therefore, the major limitation of the calculations reported here is to overestimate the weight of negative values in ΔE_4, that is, overestimate the stability of the oxidised form Cu^{II}-Aβ.

As an example of the method, in this article we analyse the energetics, at an approximate DFT level of theory, of 66 configurations obtained by 80 initial empirical models in which Cu^{2+} is bound to each peptide through Asp1, His6 and His13 (Nϵ2), and 52 configurations obtained by 55 empirical initial models in which Cu^{2+} is bound to one peptide through Asp1 and His6, and to a second peptide through Nϵ2 of His13. In all cases the experimental coordination Ia is assumed, but the position of water molecules, reactant dioxygen molecule and superoxide product in the Cu inner sphere and negatively charged side chains of Asp residues differ.

Methods Section

The methods used in this work are summarised in Figure 2. The most important information to retain in the empirical model is the set of constraints due to the peptide arrangement around each Cu site. To retain this information, the relaxation stages performed with inclusion of valence electrons in the model are short (20 steps). This is an empirical balance between the requirement to relax bond lengths and angles with a small deformation of the ligands.[23] This approximation implies that all the Cu coordination geometries sampled in the reaction pathway described in Equations (1)–(3) are those of minimal reorganisation for the resting oxidised state.

Structure preparation and MD simulation

We performed molecular dynamics (MD) simulation of a system composed of two Aβ(1–42) peptides bound in two different ways to Cu^{2+} in 1:1 ratio. The force-field parameters were those used in our previous work[20] on Cu-Aβ monomers and dimers: the usual models for water (TIP3P[24]) and NaCl[25] were applied together with the 99SB Amber force field[26] updated with parameters for Cu^{II} equatorial binding as in EPR component I (Ia). Below, we summarise the simulation procedure used in this work.

We aimed at obtaining a sample of different structures for Cu-Aβ(1–42) monomers and dimers, each characterised by: 1) the same coordination of Cu, representing the most abundant Cu^{II} coordination (see Introduction); 2) sampling of different ligand structures (monomeric and dimeric), each representing a different environment for the first Cu coordination sphere, accessible under ambient thermal conditions. In dimeric Cu-Aβ(1–42) systems, one of the two His side chains binding Cu may belong to a peptide different from that providing the other His side chain. Therefore, we built two types of Cu coordination: in the first type (set **1**, hereafter) Cu is bound to Asp1 (N and O), His6 (Nδ1) and His13 (Nϵ2), whereby all side chains belong to the same peptide (say peptide A); in the second type (set **2**, hereafter) Asp1 and His6 belong to one peptide (A), while His13 belongs to the other peptide (B). For each type of coordination (set) we aimed at differentiating the possible peptide configurations. For this purpose, we used metady-
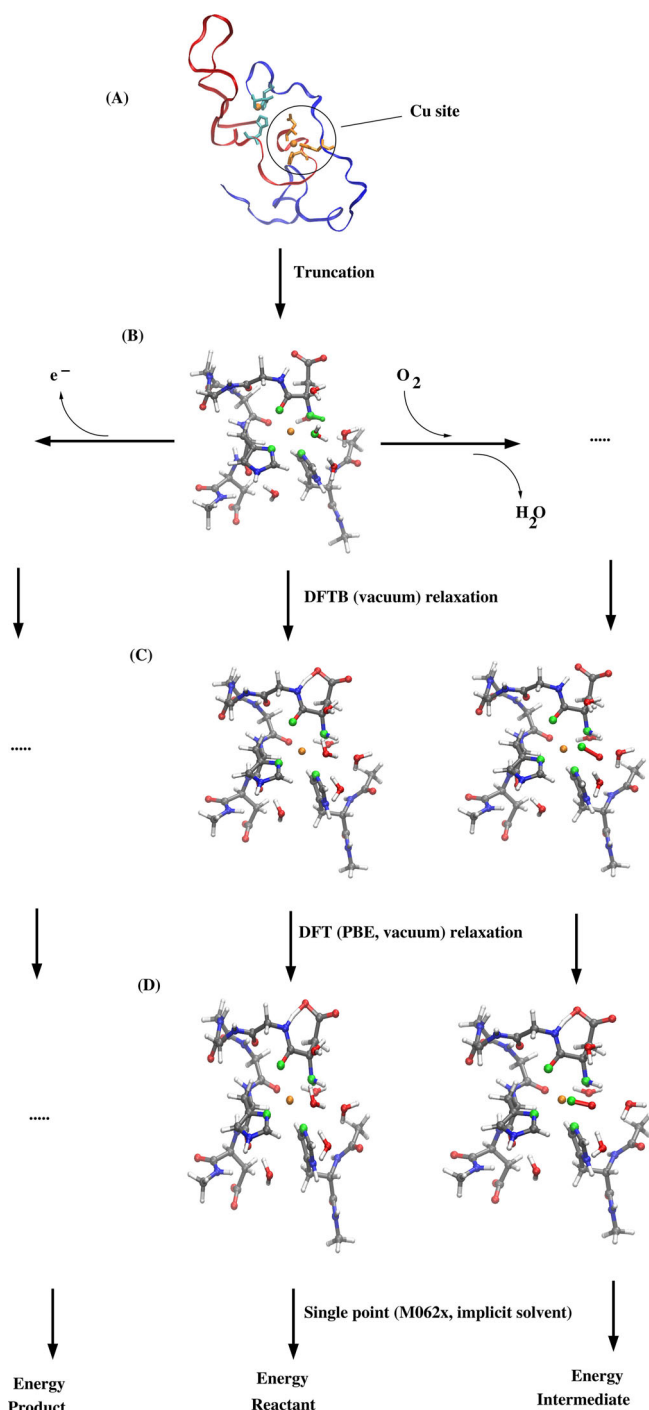
These are not the final page numbers! ↗↗

Figure 2. The methods used to reach the representative configurations of the states depicted in Figure 1. The MD simulation (A) contains a thermal bath of water molecules (not displayed), from which those within 5 Å of the Cu site are extracted (B). Atomic and bond radii are arbitrary. The VMD program[30] was used for all the molecular drawings. Atoms within 2.5 Å of the Cu site are emphasised in green. For details, see the Methods Section.

namics based on a collective variable that in our previous work[20] was found effective in changing the peptide structure, that is, the number of salt bridges (SB). This variable is the number of contacts between positively charged groups (Nη of Arg and Nζ of Lys) and negatively charged groups (Cγ of Asp, Cδ of Glu and C in C terminus). The contact is defined when the atoms of the groups are within 4 Å. We aimed to study the first Cu coordination sphere and

its reactivity in O_2 activation in peptide configurations characterised by different values of SB.

For set **1**, we extracted one configuration of Cu^{II}-Aβ(1–42) from the basin of maximal probability obtained with a microsecond-long MD simulation of Cu^{II}-Aβ(1–42) monomers,[20] which are assumed to be the resting state of any in vitro study of oxidoreductive properties of Cu complexes in the presence of dioxygen (see Introduction). To build dimers, two identical monomers were placed at a distance between geometry centres of 2 nm and randomly rotated. We chose 80 different mutual orientations as initial configurations for a multiple-walkers MD simulation[27] based on a common history-dependent bias function of SB. The latter bias was built with the recent altruistic metadynamics method.[28] Each walker is also termed a replica hereafter. The goal of the multiple walkers is to sample all values of SB in a given range (0 ≦ SB ≦ 20) while preventing different walkers from repeating sampling of values that have large degeneracy.

Each replica was simulated for 22 ns in a thermal bath of explicit water molecules and NaCl at $T = 300$ K and $P = 1$ bar. Periodic boundary conditions were used in three dimensions. The NAMD 2.10 package[29] was used for all MD simulations, and VMD[30] for analysis and visualisation. After energy minimisation, we integrated equations of motion acting on atoms using a time step of 2 fs with constraints[31] acting on bond lengths involving H atoms, a distance cut-off for nonbonding interactions of 1.1 nm and the smooth particle mesh Ewald algorithm[32] for long-range electrostatic interactions. We used stochastic thermostat[33] and barostat[34] to keep temperature and pressure, respectively, constant. The simulation cell was kept orthorhombic by the equation of motion consistent with the NPT statistical ensemble. The system representing set **1** was composed of 1252 protein atoms, 2 Cu, 31 Na, and 27 Cl atoms and 15 229 water molecules. Since configurations in set **2** have less space for water between the two peptides than those in set **1** (see below), set **2** contained 14 462 water molecules. On the other hand, the more extended peptide chains in set **2** provide a larger anisotropy to the simulation cell. Table 1 lists some of the simulation parameters and conditions used for the two sets. The parameter α indicates the weight of the histograms in altruistic metadynamics linear combination. This weight is applied to histograms that originate from walkers different from that for which the bias is used for the next simulation stage. When α is not reported, the same bias resulting from the previous stage is applied to all walkers, as is required in any final metadynamics stage. We note that our goal is not to use the metadynamics to build a free-energy profile as a function of the chosen collective variable SB. The use of metadynamics is here meant to spread walkers over different values of SB.

The construction of initial configurations for set **2** was different, because dimers are linked by interpeptide covalent bonds involving bridging Cu atoms. The first configuration built in set **1** was chosen as initial configuration for a Monte Carlo (MC) random walk in the torsional space of the peptides.[35] A similar approach was adopted in ref. [16] and described in the supplementary material provided for that work. All dihedral angles Φ and Ψ are randomly changed in the 0–360° range, while keeping Asp1 in chain A and the Cu ion bound to it fixed in space. The temperature for the Metropolis MC test, based on the potential-energy change upon configuration modification, is randomly chosen within 0 and a given maximum, 10 000 K. The reciprocal temperature $\beta = 1/RT$ is uniformly sampled in the corresponding temperature range. The MC random walk is performed until Nε2 of His13 in chain B enters into the Cu(A) coordination sphere. This condition is fulfilled when Cu(A)−Nε2 [His13(B)] is within 4 Å. We selected 20 configurations

Table 1. Parameters used in MD simulation for each walker.[a]				
Simulation stage	Ensemble	Bias	α	t [ns]
Set 1				
0	NVT	no	–	0.3
1	NPT	no	–	8
2	NPT	yes	–	2
3	NPT	yes	0.25	2
4	NPT	yes	0.50	2
5	NPT	yes	0.75	2
6	NPT	yes	1.00	2
7	NPT	yes	–	2
8	NPT	no	–	2
Set 2				
0	NVT	no	–	0.3
1	NPT	no	–	2
2	NPT	yes	–	10
3	NPT	yes	0.25	4
4	NPT	yes	0.50	4
5	NPT	yes	0.75	4
6	NPT	yes	1.00	4
7	NPT	yes	–	2
8	NPT	no	–	4

[a] Temperature T is 300 K, except in stage 0, in which it was increased from 0 to 300 K during the first 0.3 ns. In the NPT ensemble, the pressure P was kept constant at 1 bar. When α is reported, the value was used in Equation (3) of ref. [28] to build the bias used in the actual stage on the basis of the histograms of the number of salt bridges (the collective variable SB) obtained with all walkers in the previous stage. The last nanosecond of stage 8, that is, in absence of any bias, was used for RMSD analysis.

fulfilling the above condition. The same MC random walk was then repeated while keeping fixed Asp1 of chain A and Hi13 of chain B, together with Cu(A), until configurations with Nδ1 of His6(A) enter the coordination sphere of Cu(A). Once Asp1(A), His6(A) and His13(B) are all within the coordination sphere of Cu(A), the procedure is repeated with Cu(B), which was kept attached to Asp 1(B) in all MC moves. This procedure allowed the collection of 55 configurations with Cu(A) approximately coordinated by Asp 1(A) (N and O atoms), His 6(A) (Nδ1) and His 13(B) (Nε2), and at the same time Cu(B) approximately coordinated by Asp1(B), His6(B) and His13(A). The covalent bonds were then activated and the energy minimised. The 55 configurations obtained with this procedure were then used as starting points for 55 walkers (see description above for set **1**). Since the number of replicas (55) is smaller in set **1** than in set **2** (80), the MD simulation of each replica, both with and without the applied bias, was longer (34 ns, see Table 1).

On the basis of the analysis of root mean square deviation (RMSD) within the trajectory of each replica and between different final points for replicas (see Results), we chose the last collected configuration for each independent replica for further modelling including electrons.

DFTB relaxation

To include electrons, simplification of the ligand is required. This procedure is named ligand truncation. In this application the ligand is composed of amino acids, but also water molecules and dioxygen. This type of truncation scheme has been already applied to Cu-Aβ.[16] With A and B indicating the peptide chains of each monomer, residues Asp1(A), His6(A), Asp7(A), and His13(A or B) are entirely included in the following models with electrons. To keep the mechanical constraints acting on the 1–7 (A) loop, residues

Ala2, Glu3, Phe4 and Arg5 are transformed into Gly and thus retain the peptide backbone of the 1–7 region of peptide A. Where truncation of the peptide chain occurs, termini are replaced, as usual, with CH_3CO- (Ace) and $-NHCH_3$ (NHmet) groups. All water molecules with O atom closer than 5 Å to Cu were also extracted from the same MD sample.

To relax the stress due to the inclusion of valence electrons in the model, we used the Hamiltonian of the system based on the self-consistent charge density-functional tight-binding approximation[36] (DFTB). In this approximation, geometrical parameters (e.g., distances and angles) of minimal-energy conformations are consistent with accurate DFT calculations for a large set of organic molecules, both isolated and in condensed phases. We used the DFTB+ code[37] for these simulations. The valence electrons of each atom were represented as s and p orbitals; d orbitals were added to Cu. We used the parametrisation for Cu proposed for a Cu complex similar to Cu-Aβ.[38]

Each configuration extracted from the empirical stage was minimised for 20 steps. This relaxation step has the major advantage of relaxing the terminal groups replacing the truncated residues in the peptide.

DFT relaxation

We used the parallel version of the Quantum-Espresso package[39] to further reduce the atomic forces in the geometries obtained with the DFTB approximation. The DFT approximation is here designed to speed up the calculations; therefore, it involved the Vanderbilt ultrasoft pseudopotentials[40] and the PBE exchange-correlation functional.[41] Electronic wave functions were expanded in plane waves up to an energy cut-off of 25 Ry, while a 300 Ry cut-off was used for the expansion of the augmented charge density in the proximity of the atoms, as required in the ultrasoft pseudopotential scheme. We inserted each configuration in a cubic supercell of 30 Å, suitable to avoid interactions between periodic images of Cu model complexes. After 20 steps of energy minimisation, performed with the Broyden–Fletcher–Goldfarb–Shanno algorithm, the atomic forces never had any component larger than 0.01 Ry bohr^{-1}.

Single-point calculations

This step provides the energy values used to compute the energy changes for reactions in Equations (1)–(4) (see Figure 1). We used the Gaussian 09[42] code for the single-point calculation of energy for the final atomic configurations obtained in the previous DFT relaxation stage. The DFT set-up, identical to that used in ref. [7], includes a localised basis set of type 6-31+G(d) for N, O, C and H atoms, and LANL2DZ for Cu, the atomic core of which is described by a pseudopotential. We used the M06-2X hybrid exchange functional,[43] which was found to be suitable to describe the second ionisation energy of Cu and the electron affinity of dioxygen. The latter parameters are the basis of the charge transfer in $Cu^{II}\cdots O_2^{\bullet-}$ species [Eq. (2a)]. We modelled the solvent effects, only at this stage, with an implicit polarizable continuum model (SMD).[44] The geometries of O_2, O_2^- and H_2O were optimised at the same level of DFT approximation.

The atomic charge density was determined by natural bond order population analysis,[45] and the corresponding atomic charge is denoted q.

Not all of the configurations satisfy a ground-state electron wave function, since convergence is not achieved in a small amount of configurations produced with the more approximate PBE exchange

functional. The critical step is the unrestricted calculation of the Cu-Aβ-(O$_2$) ternary complex (intermediate) in the triplet state. For this system, 66 of 80 configurations converged to the ground state in set **1**, and 52 of 55 in set **2**. For configurations representing reactant, 78 of 80 configurations converged in set **1**, while all configurations converged for set **2**. For configurations representing product, 79 of 80 configurations converged in set **1**, and 54 of 55 for set **2**.

Structural parameters

Hydrogen bonds were defined as present when the X⋯Y distance in XHY is shorter than 3 Å and the X—H⋯Y angle is larger than 135°. The solvent-accessible surface area (SASA) was determined[46] by using atomic radii for amino acids.[47] The radius of Cu was set to 1 Å. Electron units were used for atomic charges.

The extent of complex formation in set **1** was measured by the ratio R between the SASA of the assembly and the sum of the SASAs of the two monomers A and B [Eq. (9)]. The assembly is assumed to be a dimer if $R < 0.95$.

$$R = \text{SASA}([A-B])/[\text{SASA}(A-B) + \text{SASA}(B)] \qquad (9)$$

The coordination number (CN) is defined as the number of atoms within a given distance cut-off from Cu. In this work the cut-off for the distance was 2.5 Å. Once the coordination number CN is determined and the ligand atoms L are identified, the geometry of the coordination is measured by means of the eigenvalues of the ordering matrix formed with the coordination bonds Cu—L. The ordering (or Saupe) matrix is defined as Equation (10):

$$Q_{\alpha,\beta} = \frac{1}{2}\left[\frac{3}{\text{CN}} \sum_{i=1}^{\text{CN}} \vec{u}(i)_\alpha \vec{u}_\beta - \delta_{\alpha,\beta} \right] \qquad (10)$$

in which $\vec{u}(i)$ is the unitary vector along each Cu—L bond, δ is the Kronecker symbol, α and β run over the three directions of space and i runs over the ligand L atoms. The three eigenvalues of the ordering matrix are compared with the exact eigenvalues determined for the ideal coordination geometries (linear, trigonal, tetrahedral, etc.). The geometry is identified as one of the exact geometries when the RMSD between the calculated eigenvalues and the exact eigenvalues is within 1/4.

Results

Structural deviations among collected samples

Before reporting the calculations of the energy changes ΔE_2, ΔE_3 and ΔE_4 in Equations (2), (3) and (4), respectively, we first characterised the structures of the 135 samples (80 for set **1** and 55 for set **2**) that were used for the analysis of energetics.

For disordered proteins such as Aβ, the length of a single simulation that is able to sample a stationary ergodic process is beyond the microsecond timescale. The simulation protocol we applied here is designed to obtain Aβ ligand configurations representing different host peptide structures for the guest Cu active site, all accessible under ambient thermal conditions. The achievement of reliable statistical weight of configurations is still beyond the possibility of computational methods.

Since each trajectory was simulated in the NPT statistical ensemble, the sides of the orthorhombic cell L_x, L_y and L_z are variable quantities. Cell sides decrease at the beginning of the NPT simulation (stage 2 in Table 1) to accommodate the water solvent and the ionic atmosphere around each initial configuration. After this settling, the fluctuation of the variables is always within 0.1 Å. The variation of cell sides between different walkers is larger, as shown in Figure 3, in which the averag-
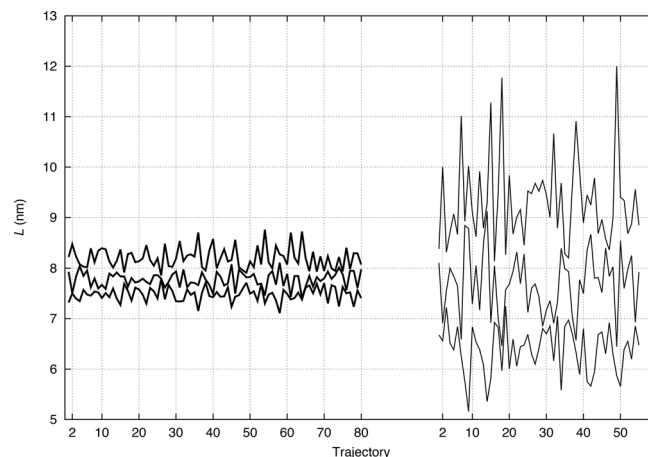

Figure 3. Average over each MD trajectory of the orthorhombic cell sides L_x, L_y and L_z. Set **1** is on the left-hand side, and set **2** on the right-hand side. Root mean square errors are always smaller than 0.007 and 0.01 nm for sets **1** and **2**, respectively.

es of the cell sides are shown for the last stage of simulation. Particularly for set **2**, the cell anisotropy is significant. This effect is due to the construction of initial configurations. Monte Carlo random walks, used to build initial configurations in set **2**, produce extended peptide-chain configurations that are expected to slowly relax during the MD simulations. This effect has been partially circumvented in set **1**, because initial monomers were obtained by long MD simulations, and therefore they are more compact from the beginning. In any case, there are no direct interactions between different periodic replicas of the solute, that is, no atomic pairs involving periodic replicas of solute are within the distance cut-off used for nonbonding (Lennard–Jones and direct Coulomb) interactions (1.1 nm, see Methods Section).

Since the empirical force field for Cu^{II}-Aβ interactions is designed to represent the Cu coordination consistent with **Ia** geometry in the oxidised state (EPR component I), the main differences between Cu coordination samples is in the access of water to Cu from a axial direction with respect to the four equatorial ligands. Figure 4 shows the RMSD[48] computed for the final points of the different walkers, by using the first walker of each set as reference (thick line). This RMSD is compared with the RMSD evaluated during the last nanosecond of each trajectory (thin line), by using the final point of the respective trajectory as reference. The RMSD computed for all peptide atoms (Figure 4 A) and that computed for the ligand atoms used as truncated models when electrons are included (Figure 4 B) are shown. In both panels the larger RMSD for the configurations of set **2** shows that the condition of imposing a Cu bridge between two monomers exerts significant con-
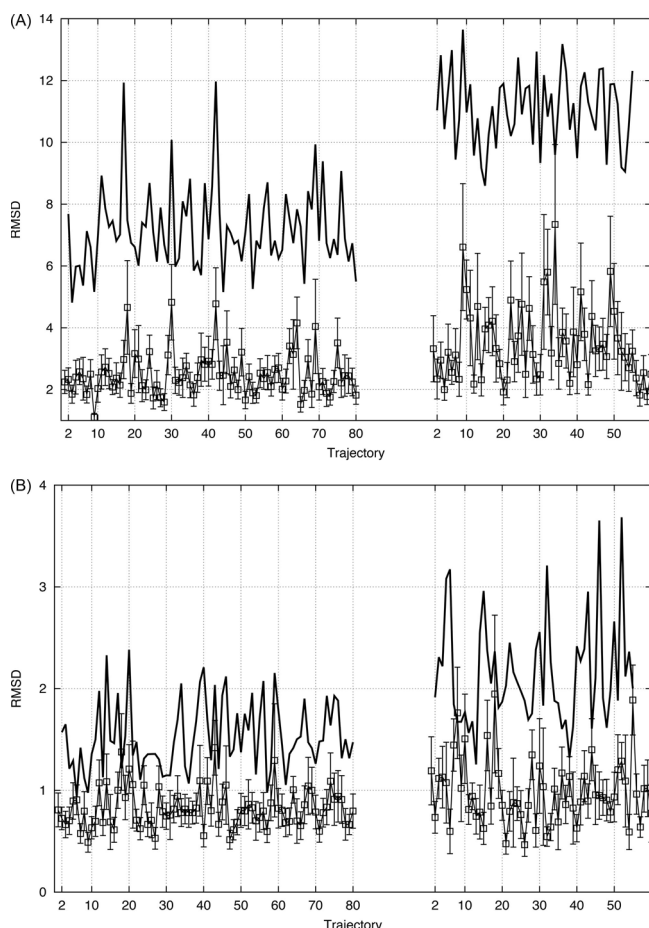
Figure 4. RMSD within final points obtained by different walkers (thick line, reference is the first walker) and obtained within the last ns of MD simulation of each walker (thin line, error bars display root-mean square errors, reference is the final configuration). A) RMSD computed for all protein atoms of monomer A. B) As for A) but computed for the atoms representing the Cu ligand (Asp 1(A), backbone of residues 2–5 of monomer A, His6(A)-Asp7(A), His13(A/B)). Results for walkers 1–55 are shown on the right-hand side of each plot).

straints both on the entire monomer and on the Cu ligands. The comparison between the two panels shows that the distortions of the Cu coordination (excluding the water molecules in the vicinity of Cu) are only in a few cases of set **2** larger than 3 Å, that is, a value that was assumed as a threshold for distinguishing structures (Figure 4 B). The RMSD of monomer A (Figure 4 A) is, on the other hand, larger than 3 Å when different final points are compared to the final point of the first trajectory (solid line). The RMSD within the last nanosecond is, in most of the trajectories, smaller than 5 Å. These comparisons indicate that the final points of each trajectory represent a wide spectrum of configurations for monomer A (from which the Cu site is extracted in all cases). All of these points are accessible under ambient thermal conditions, even though the statistical weight of configurations cannot be computed with this method, because the simulations are too short in time and the number of walkers is too small.

Although the Cu-site configurations sampled differ only slightly in the geometry of the ligand atoms, the differences in

many structural parameters concerning the Cu environment are large. The number of samples that represent Cu^{II}-Aβ dimers, according to a threshold of $R < 0.95$ (see Methods Section), is 30 of 80 in set **1**. This shows that the sampling performed with metadynamics allows both monomeric and dimeric states to be investigated under ambient thermal conditions.

Table 2 summarises the distribution of some of the relevant structural parameters dealing with the Cu environment, focusing on the state of water molecules and dioxygen reactant in the vicinity of the Cu atom. These parameters were computed

Table 2. Number of configurations fulfilling selected structural conditions among all samples used for reactant (78 + 55), intermediate (66 + 52) and product (79 + 54) states in the two coordination types (sets **1** and **2**).[a]

Set	State	d(Cu—O)	HBd = 0	HBd = 1	HBd = 2	HBa = 0	HBa = 1	HBa = 2
1	reactant	15	0	3	12	2	10	3
	intermediate	60	–	–	–	57	3	0
	product	27	0	7	20	6	17	4
2	reactant	8	0	3	5	2	4	2
	intermediate	37	–	–	–	33	4	0
	product	19	0	9	10	6	9	4

[a] d(Cu—O): distance between Cu and the closest water molecule (or O in dioxygen) is shorter than 2.5 Å, that is, water (or dioxygen) is bound to Cu. HBd = 0: water molecule is bound to Cu and donates no hydrogen atoms as hydrogen bonds. HBd = 1: water molecule is bound to Cu and donates one hydrogen atom as hydrogen bond. HBd = 2: water molecule is bound to Cu and donates two hydrogen atoms as hydrogen bonds. HBa = 0: water (dioxygen) molecule is bound to Cu and accepts no hydrogen atoms as hydrogen bonds. HBa = 1: water (dioxygen) molecule is bound to Cu and accepts one hydrogen atom as hydrogen bond; HBa = 2: water (dioxygen) molecule is bound to Cu and accepts two or more hydrogen atoms as hydrogen bonds.

for the configurations analysed in single-point DFT calculations, that is, the structures representing the energetics of the reactions in Figure 1. Most of the water molecules bound to the Cu centre are involved in hydrogen bonds with other groups, mainly other water molecules in the site. The number of hydrogen bonds involving the Cu-bound water molecules increases with increasing oxidation state of Cu, consistent with the higher water polarisation measured by atomic charges (data not shown) and with the number of samples characterised by short Cu—O distances. For dioxygen close to Cu^{I} (see below for the characterisation of the intermediate state), most of the configurations represent possible Cu-bound states, with a few hydrogen bonds involving dioxygen. These data show that the sampled configurations represent different contributions to the description of the reactant (Cu^{I}), intermediate and product (Cu^{II}) states due to the interactions in the axial region of the Cu site described here.

Charge separation in the intermediate state

The intermediate state is described by 118 samples in which the convergence of the ground-state electron density was successful: 66 of 80 in set **1** and 52 of 55 in set **2**. The first ques-

tion that can be answered with the many configurations collected is the chance for configurations to show a contribution of electron transfer $Cu^{II}\cdots O_2^{\bullet-}$ to the ground-state electron density. This measure is provided by the atomic charge derived by the natural population analysis. The atomic population summed over the two O atoms in O_2 never shows an excess of electrons below 0.7 in set **1**, while in set **2** there are four configurations with excess charge on dioxygen lower than 0.2. Therefore, the superoxide electron configuration $Cu^{II}\cdots O_2^{\bullet-}$ contributes to the ground state of dioxygen when it is coordinated in the inner sphere of the Cu centre, as in the **Ia** geometry, with a few exceptions (4 of $118 = 66 + 52$ configurations in which the ground-state electron density converged).

Energy change with reactions

Since the initial configurations for DFT relaxation were obtained by MD simulations of empirical models in the resting oxidised state Cu^{II}-$A\beta_{42}$, the Cu coordination starts from coordination number four (the equatorial ligands), and in some cases five, because of the approach of water molecules from the axial direction (see Table 2 for reactant species). Nevertheless, during the DFT relaxation in the reduced state [reactant species in Eq. (2)], the distances between the Cu and ligand atoms in the equatorial plane of the Cu^{II} initial geometry change significantly on Cu reduction. In Table 3, the range of sampled distances and geometries is reported for reactant and product states. In the reactant state the Cu—O(Asp1) distance shows deviations beyond 2.5 Å: the number of samples in which this distance is larger than 2.5 Å is 24 of the 78 converged samples of set **1**, and 22 of the 55 samples of set **2**. The Cu—Nε(His13) distance is larger than 2.2 Å in four of 80 samples and seven of 55 samples in sets **1** and **2**, respectively, and this shows that in

Cu-bridged dimers significant mechanical constraints act on the Cu environment.

The extent of structural diversity obtained with relaxation in both reactant and product states is summarised in Table 3 for the distribution of samples with ideal geometries available to Cu (see Methods Section). Even though concentration of the samples for square-planar coordination number four is shown, there are both three-coordinate T-like configurations in the reactant state and five-coordinate trigonal-bipyramidal geometries in the product state. The $n(CN = 5)/n(CN = 4)$ ratio in the product state and $n(CN = 3)/n(CN = 4)$ ratio in the reactant state are larger in set **2** than in set **1**. This shows that an ideal square-planar coordination of Cu^{II} is more easily realised when Cu bridges two peptides than in a Cu site wrapped by a single $A\beta$ chain.

The energy change ΔE_4 for Cu oxidation [Eq. (4)] is shown in Figure 5 as a function of the Cu—O(Asp1) distance in the reactant species. The CN, that is, the number of ligand atoms within 2.5 Å of the Cu centre (including water molecules), is also displayed, as it is calculated in the reactant species. We as-
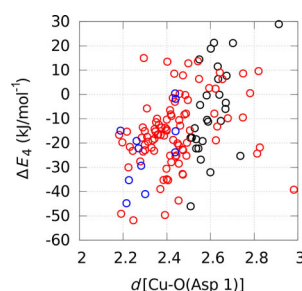

Figure 5. Values of ΔE_4 (y axis) as a function of the distance between Cu and O (Asp1), measured in configurations representing the reactant reduced state (see Figure 1). Blue points are configurations with Cu CN = 5, red points CN = 4 and black points CN = 3. Both sets (78 samples for **1** and 55 for **2**) are displayed.

Table 3. Summary of Cu coordination geometry in reactant (Cu^I) and product (Cu^{II}) species in sets **1** and **2**.[a]

	Set **1** react.	Set **1** prod.	Set **2** react.	Set **2** prod.
Cu—N(Asp1)	2.03–2.27	2.03–2.14	2.01–2.35	2.03–2.18
Cu—O(Asp1)	2.22–2.92	2.05–2.60	2.18–2.98	2.05–2.79
Cu—Nδ(His6)	1.93–2.09	1.97–2.10	1.93–2.09	1.97–2.08
Cu—Nε(His13)	2.01–2.31	2.04–2.18	2.04–2.42	2.04–2.25
n(tbp)	7	25	1	19
n(sqp)	48	52	29	30
n(tp)	7	1	7	4
n(T)	15	0	12	0
n(nc)	1	1	2	1
$n(CN = 3)$	15	0	12	0
$n(CN = 4)$	56	53	38	35
$n(CN = 5)$	7	26	5	19
n	78	79	55	54

[a] Range of distances [Å] between Cu and equatorial ligands; number of samples n with coordination geometry specified as sqp (square planar), trigonal-bipyramidal (tbp), trigonal-based pyramidal (tp), or T (T-like); nc means that the geometry cannot be classified as tetrahedral or trigonal (see Methods Section). Ligand atoms are N(Asp1), O(Asp1), Nδ(His6), Nε(His13), O(water), and Oδ(Asp1). CN is the number of ligand atoms within 2.5 Å of the Cu site. The total number of samples is n (last row).

sociate a different colour with each of the represented values of CN (3, 4 or 5). A value of CN = 3 represents configurations in which the O(Asp1) atom is remote from the Cu centre and neither water molecules nor Oδ of Asp1 can bind to the Cu centre. A value of CN = 5 represents configurations that do not change, upon reduction, from the high CN of 5 typical of Cu^{II} in the resting oxidised state of a disordered Cu^{II}-$A\beta$ peptide, with the Cu site accessible to water molecules. We define the latter condition as Cu crowding, because under this condition it is not easy for the peptide ligand and its solution environment to remove a large number of potential ligand atoms around Cu, and thus destabilise the oxidised state.

In Figure 5, small values of ΔE_4 are, as expected, found for high values of CN (blue points), but also lower CNs contribute. Even though the distribution of energy is wide, the largest values of ΔE_4 are found for CN = 3 and for Cu—O(Asp 1) distances larger than 2.6 Å. Angular distortions of Cu bonds do not contribute to increase the values of ΔE_4. We remark that Oδ(Asp 1) is also involved in Cu coordination (see below). Such interaction explains, for instance, the point with Cu—O(Asp1)
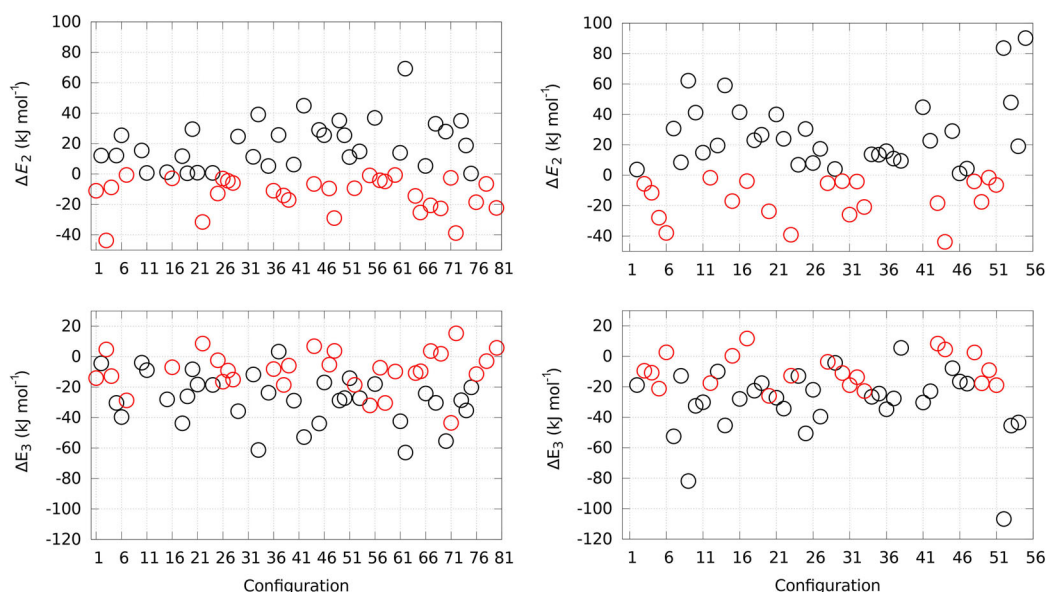
↖↖ **These are not the final page numbers!**

Figure 6. Values of ΔE_2 (top) and ΔE_3 (bottom) for reactions in Figure 1 [Eqs. (2) and (3)], and for the 118 configurations representative of the intermediate state (66 for first set, left panel and 52 for the second set, right panel). Points with positive values of ΔE_2 are in black, and negative values in red.

distance of 3 Å, $\Delta E_4 = -40$ kJ mol^{-1} and CN = 4 in Figure 4. This shows that Oδ(Asp1) can efficiently replace O(Asp1), but this interaction stabilises the oxidised state of Cu.

The energy change for reaction 2 [ΔE_2, i.e., ΔE of Eq. (2)] provides an estimate of the free-energy change for climbing from reactant to the eventual intermediate state mostly represented by the Cu-bound superoxide. The values computed for sets of configurations **1** and **2** are separately displayed at the top of Figure 6 (left and right panels, respectively). The Cu-bound dioxygen states (the four triplet dioxygen states found in the second set of configurations, i.e., configurations 9, 41, 52 and 55 in the right panel) have positive values of ΔE_2.

In both sets, about one-half of the configurations show negative values of ΔE_2, that is, the production of a superoxide anion confined within the Cu inner sphere (within 5 Å of Cu) is not sufficiently hindered, neither by Cu coordination constraints or by the peptide wrapping around Cu. Also, the significant distortions of the ligand peptide occurring in set **2** (Figure 6) do not inhibit significantly the formation of superoxide.

The bottom panels of Figure 6 show the ΔE_3 values, while keeping track of points that show a negative value for ΔE_2. The points for which both energy changes are negative represent downhill processes for the oxidation of Cu together with the formation of superoxide outside of the Cu inner sphere. There is a strong anticorrelation between the signs of ΔE_2 and ΔE_3, showing that the state denoted "Intermediate" in Figure 1 is, in many of the probed configurations, a real intermediate state. When ΔE_2 is negative and ΔE_3 is positive, the state is easily reached when dioxygen penetrates the inner sphere of Cu^I, but superoxide is not easily released into the Cu outer sphere. Under these conditions, the Cu site can rearrange to better host Cu^I, and thus the potential for the reduction of Cu^{II} is decreased. Under the latter conditions, dioxygen can be recovered because of settling of the Cu^I coordination.

About one-fourth of the configurations in both configuration sets have negative values of ΔE_2 and ΔE_3. Most of the red points in the bottom panels (i.e., configurations with negative values of ΔE_2) have ΔE_3 between zero and -20 kJ mol^{-1}. We searched for triplets of values that can represent easy turnover of the reactant (the reduced Cu-Aβ complex, that is, a small energy change for Equation (1). This "ideal" case is represented by negative values for ΔE_2 and ΔE_3, together with a value of ΔE_4 within a small range, for example, $-20 < \Delta E_4 < 0$. This search found 15 cases among the 118 samples. Again, this shows a high chance for the production of superoxide, its ejection into the protein environment and a low energy requirement for the production of the initial reactant.

Table 4 lists the distances between the Cu centre and its ligand atoms for the three states on the pathway that displays the flattest profile of ΔE changes. The structure of the reactant state is shown in Figure 7. Superoxide easily replaces the water molecule in the axial coordination site of reduced Cu, since the axial water molecule is farther than 2.5 Å from the Cu centre. The distances between Cu and N/O of Asp1 decrease with oxidation of Cu by dioxygen. Then, the distances are maintained

Table 4. Cu–ligand distances along the reaction pathway for configuration 53 of set **1**.[a]

Distance	Reactant	Intermediate	Product
N(Asp1)—Cu	2.14	2.12	2.09
O(Asp1)—Cu	2.36	2.37	2.08
Nδ1(His6)—Cu	2.03	2.05	2.04
Nε2(His13)—Cu	2.09	2.11	2.06
O$_{ax}$—Cu	2.82	2.03	2.55

[a] O$_{ax}$ in the intermediate state is the superoxide O atom closest to Cu, while it is O of water in reactant and product. $\Delta E_2 = -5$, $\Delta E_3 = -4$, $\Delta E_4 = -9$ kJ mol^{-1}. See Figure 1 and Equations (2)–(4) for the meaning of the quantities.
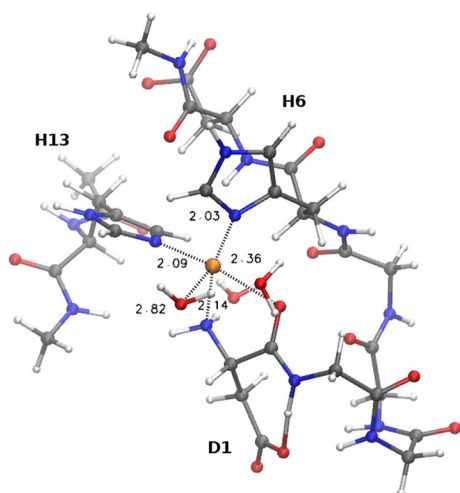
Figure 7. Structure of the reactant on the pathway of configuration 53 in set **1**. The distances between Cu and its ligand atoms are displayed. The evolution of these distances is reported in Table 4.

when superoxide is replaced by water, which is bound to the Cu centre axially, as in the stable square-pyramidal Cu^{II} coordination environment. The slight displacement of equatorial ligands, together with the light push-and-pull movement of the axial water molecule, represents a small reorganisation of the Cu site that hosts both oxidation states and the dioxygen electron shuttle. This flat energy pathway is an alternative to pathways that involve displacement of O(Asp1) from the Cu centre,[8,22] which involves a higher reorganisation energy. The data concerning ΔE_4 clearly show that the displacement of ligands from the equatorial plane of Cu^{II}-Aβ is required to obtain Cu^{I}-Aβ by oxidising either ascorbate or superoxide. Indeed, the largest value of ΔE_4 in Figure 5 ($\Delta E_4 = 30$ kJ mol^{-1}) is associated with a Cu site having three ligands, with Nδ(His6) *anti* to N(Asp1) and Nϵ(His13) binding from the orthogonal direction, and thus represents T-like coordination of Cu^{I}. This coordination mode has been already addressed as a good candidate for efficient Cu reduction. In the case of dioxygen activation, this geometry is not active, because $\Delta E_2 = 26$ kJ mol^{-1} and $\Delta E_3 = 3$ kJ mol^{-1}. This is due to the repulsion of water molecules *anti* to Nϵ(His13) and to the low chance to attract dioxygen from the same direction. Therefore, a fine balance in Cu plasticity upon reduction is required by the proposed reaction mechanism. A study including a wider model of the ligand reorganisation around Cu will be the next step to better describe its catalytic role in ROS production.

The hydrogen bond between the carboxylate group of Asp1 and HN of Ala2 is displayed by most of the configurations collected in this work. This hydrogen bond activates the binding of Cu by O(Asp1), and thus prevents the release of such a bond upon Cu reduction. In a few configurations the carboxylate group of Asp1 enters the first coordination sphere of Cu (d(Cu–Oδ) $\leq$ 2.5 Å). This event occurs in the reactant state for one configuration in set **1** (78 samples) and for seven configurations in set **2** (55 samples). The chance for interactions between Cu and the Asp1 carboxylate group has been addressed as an important contribution to the electron transfer to dioxy-

gen.[2,7] Also, the greater chance for Oδ(Asp1) to enter Cu coordination when different Aβ peptides are bridged by Cu has been observed in previous structural models. However, the set of configurations analysed in this work do not contain configurations in which one of the His side chains breaks the bond with Cu, as is observed in previous works.[7] Thus, the effect of carboxylate on the oxidised state of Cu^{II}-Aβ cannot be fully exerted, and the ΔE_2 values for these are positive in five of eight cases in which Oδ(Asp1) approaches the Cu centre. This limited exchange of ligands around Cu will be removed in future works, and thus the exploitation of reaction steps characterised by high reorganisation energy enhanced. In terms of truncated models, some of these configurations have been studied in the reduced state Cu^{I}-Aβ.[22]

It is important to search for geometrical parameters, such as those reported in Tables 2 and 3, that correlate with the sign of ΔE_2, and thus indicate whether there is a specific interaction that can favour or disfavour, for instance, step 2 in the proposed mechanism. Interestingly, the minimal distance between O$_2$ and Cu is not strongly correlated with the sign of the energy change ΔE_2. For instance, in set **1** there are five configurations in which the Cu–O distance is longer than 3 Å, but two of these configurations have $\Delta E_2 < -20$ kJ mol^{-1}. This shows that the charge transfer is energetically favoured even at Cu–O distances for which a Cu–O covalent bond is absent.

Despite the wide spectrum of geometries (see Tables 2 and 3) associated with the 135 probed configurations, the search for a single or a few geometrical parameters affecting the stability of superoxide in the Cu site does not provide any strong correlation with the energy change. The average Cu–L$_{eq}$ distance, where L$_{eq}$ indicates any of the four ligand atoms in the equatorial plane (N and O of Asp1, Nδ1 of His6 and Nϵ2 of His13 of chain A or B), is slightly correlated with ΔE_2, as shown in Figure 8. Even though there are exceptions, this plot shows that the closer to Cu the equatorial ligand atoms are, the lower is the energy change to produce superoxide. Since the four ligand atoms are affected by significant distortions, but are in all cases at bonding distance from Cu, the presence of these ligand atoms stabilises the oxidised state of Cu compared to the reduced state (see the above discussion concerning ΔE_4).
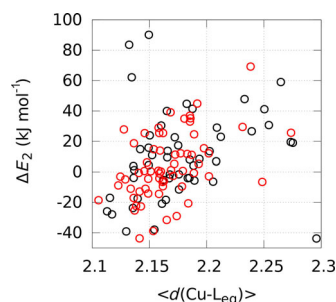

Figure 8. Values of ΔE_2 (y axis) as a function of the average distance between Cu and equatorial ligand atoms [N,O (Asp1), Nδ1 (His6), Nϵ2 (His13 A/B)] in configurations representing the reactant reduced state (see Figure 1). Red points are configurations obtained from set **1**, and black points those from set **2**.

◤◤ These are not the final page numbers!

We note that, within the approximations of the sampling reported in this work, the expulsion of the electron from the reduced Cu^I site towards dioxygen is mainly forced by the ligand atoms kept in the equatorial plane of Cu. The concentration of samples with approximately square-planar Cu coordination (Table 3) stabilises the oxidised Cu^{II} site and destabilises the reduced Cu^I site, which is suitable for more isotropic coordination or lower coordination numbers. The reported model is more focused on mimicking the presence of a nearby electron acceptor (e.g., dioxygen approaching from the water solvent), an event that is essential for the generation of ROS.

The oxidised form of Cu-Aβ (Cu^{II}-Aβ) must not be stable, to allow the Cu reduction and restore the conditions for transferring electrons to dioxygen (the reactant state). The positive sign of ΔE_4 (reaction 4 in Figure 2) means that superoxide can be transformed back into dioxygen by Cu^{II}-Aβ. This condition holds for 11 of 77 converged (in both oxidation states) configurations of set **1** and 12 of 55 of set **2**. The distribution of ΔE_4 (Figure 5) shows that Cu is easily oxidised, but superoxide has a significant chance to reduce Cu^{II}-Aβ to Cu^I-Aβ, restoring dioxygen and the possibility of superoxide production. This event can occur either with a small reorganisation of the Cu site, that is, the transition from one configuration to another among those sampled here, or, more likely, with superoxide approaching a Cu-Aβ oligomer with suitable structure in solution. The sampling provided by this computational method shows that 1/10 of the collected configurations satisfy the constraints for a partially self-sustaining cycle of reactions 2–4. This condition is met because of the structural disorder of the Aβ$_{42}$ peptide.

The main limit of the method is in the unknown statistical weight of the samples that have been chosen as representative of the energetics in the proposed reaction pathway. More extended metadynamics simulations are required to converge towards reliable statistical weights. The latter are dominated by interactions between the peptides and the environment and between peptides. These interactions are characterised by long timescales that are not yet accessible when disordered peptides are concerned. Assuming that the statistical weight of all the samples is the same, we obtain -20 ± 20 kJ mol^{-1} as the average of ΔE_4, with error calculated as the root-mean square error of collected data. The aim of this work is to show that for 135 samples that are wobbling at room thermal conditions around a given structure for 1 ns, by starting from thermally accessible configurations obtained by multiple-walkers metadynamics, the formation of superoxide is observed in all cases with the exception of four.

Conclusions

We applied a method to approximately rank the energy change of chemical steps in a hypothetical reaction mechanism involving electron transfer from reduced Cu^I-Aβ complex to dioxygen forming the aggressive ROS superoxide, which is ejected into the protein environment of the complex.

On the basis of the investigation of 135 samples characterised by significant distortions with respect to ideal geometries

and by a wide spectrum of interactions concerning the molecules (water or dioxygen) approaching the axial coordination site of the Cu atom, we conclude that the formation of superoxide has a high chance to occur once a small population of high-energy reduced Cu^I-Aβ complex is formed. In this model, the production of superoxide is allowed by the solvent accessibility to Cu from the axial direction orthogonal to the plane formed by slightly reorganising the equatorial ligand atoms. The electron transfer from Cu^I-Aβ to dioxygen is then favoured by the stability of square-planar Cu^{II} geometry in the product state, together with the low (though significant) chance to decrease the Cu coordination number to three when the complex is in the reduced reactant state. Under these conditions, the distance between Cu and the closest O atom in dioxygen can be larger than 3 Å, but still with effective electron transfer. The set of properties suitable for efficient electron transfer to dioxygen hold for a small population of high-energy Cu^I-Aβ reactant species, prior to reorganisation processes that stabilise a more redox-silent linear His-Cu^I-His coordination. Indeed, it has been shown in previous works[15] that the linear and stable His-Cu^I-His coordination of Cu^I-Aβ is more hydrophobic than Cu^{II}-Aβ.

The model also shows that part of the reduced Cu^I-Aβ reactant can be restored by oxidation of superoxide to dioxygen, and this contributes, with ascorbate, to sustaining the process of ROS production. The dual role of reductant when Cu^{II}-Aβ is more stable, and oxidant when Cu^I-Aβ is more stable, involves the structural diversity of the Cu-Aβ complex due to ligand disorder.

These observations are limited by the choice of initial configurations, largely biased by the resting oxidised state Cu^{II}-Aβ. Since the proposed method is suitable to extract mechanistic information for a large number of atomic configurations, a larger extent of distortions around the reduced state must be investigated in more detail, and this will be the continuation of this study. In this respect, the empirical MD simulation of fluxional models of Cu, both in reduced and oxidised states, appears to be the best strategy to extend the statistics. These future studies will introduce wider fluctuations of geometrical parameters acting on the electronic ground structure of Cu in both oxidation states. For instance the replacement of one His side chain by water, dioxygen or a carboxylate group can be introduced, as well as a further decrease in CN, especially in the reactant reduced state.

Also, further work is required to devise a robust method to estimate the statistical weight of the peptide assembling around one or even more Cu ions. This is particularly relevant, because this study shows that dimeric states exert mechanical forces that induce important coordination distortions on the Cu site and thus modulate its catalytic properties.

These are not the final page numbers! ↗↗

Conflict of interest

The authors declare no conflict of interest.

[1] K. Reybier, S. Ayala, B. Alies, J. a. V. Rodrigues, S. Bustos Rodriguez, G. La Penna, F. Collin, C. M. Gomes, C. Hureau, P. Faller, *Angew. Chem. Int. Ed.* **2016**, *55*, 1085–1089; *Angew. Chem.* **2016**, *128*, 1097–1101.

[2] C. Cheignon, M. Jones, E. Atrian-Blasco, I. Kieffer, P. Faller, F. Collin, C. Hureau, *Chem. Sci.* **2017**, *8*, 5107–5118.

[3] A. Quist, I. Doudevski, H. Lin, R. Azimova, D. Ng, B. Frangione, B. Kagan, J. Ghiso, R. Lal, *Proc. Natl. Acad. Sci. USA* **2005**, *102*, 10427–10432.

[4] M. Rózga, W. Bal, *Chem. Res. Toxicol.* **2010**, *23*, 298–308.

[5] C. Cheignon, M. Tomas, D. Bonnefont-Rousselot, P. Faller, C. Hureau, F. Collin, *Redox Biol.* **2018**, *14*, 450–464.

[6] D. F. Raffa, R. Gomez-Balderas, P. Brunelle, G. A. Rickard, A. Rauk, *J. Biol. Inorg. Chem.* **2005**, *10*, 887–902.

[7] A. Mirats, J. Alí-Torres, L. Rodriguez-Santiago, M. Sodupe, G. La Penna, *Phys. Chem. Chem. Phys.* **2015**, *17*, 27270–27274.

[8] T. Prosdocimi, De L. Gioia, G. Zampella, L. Bertini, *J. Biol. Inorg. Chem.* **2016**, *21*, 197–212.

[9] S. C. Drew, C. L. Masters, K. J. Barnham, *J. Am. Chem. Soc.* **2009**, *131*, 8760–8761.

[10] P. Dorlet, S. Gambarelli, P. Faller, C. Hureau, *Angew. Chem. Int. Ed.* **2009**, *48*, 9273–9276; *Angew. Chem.* **2009**, *121*, 9437–9440.

[11] D. F. Raffa, G. A. Rickard, A. Rauk, *J. Biol. Inorg. Chem.* **2007**, *12*, 147–164.

[12] J. Shearer, V. A. Szalai, *J. Am. Chem. Soc.* **2008**, *130*, 17826–17835.

[13] R. A. Himes, G. Y. Park, G. S. Siluvai, N. J. Blackburn, K. D. Karlin, *Angew. Chem. Int. Ed.* **2008**, *47*, 9084–9087; *Angew. Chem.* **2008**, *120*, 9224–9227.

[14] C. Hureau, V. Balland, Y. Coppel, P. L. Solari, E. Fonda, P. Faller, *J. Biol. Inorg. Chem.* **2009**, *14*, 995–1000.

[15] S. Furlan, C. Hureau, P. Faller, G. La Penna, *J. Phys. Chem. B* **2010**, *114*, 15119–15133.

[16] G. La Penna, C. Hureau, O. Andreussi, P. Faller, *J. Phys. Chem. B* **2013**, *117*, 16455–16467.

[17] L. Guilloreau, S. Combalbert, A. Sournia-Saquet, H. Mazarguil, P. Faller, *ChemBioChem* **2007**, *8*, 1317–1325.

[18] T. D. Rae, P. J. Schmidt, R. A. Pufahl, V. C. Culotta, T. V. O'Halloran, *Science* **1999**, *284*, 805–808, transport of Cu within cell via high-affinity Cu-binding proteins.

[19] L. Pickart, J. M. Vasquez-Soltero, A. Margolina, *BioMed Res. Int.* **2015**, *2015*, 648108.

[20] P. D. Q. Huy, Q. V. Vuong, G. La Penna, P. Faller, M. S. Li, *ACS Chem. Neurosci.* **2016**, *7*, 1348–1363.

[21] G. La Penna, C. Hureau, P. Faller, *Mol. Simul.* **2015**, *41*, 780–787.

[22] A. Mirats, J. Alí-Torres, L. Rodríguez-Santiago, M. Sodupe, *Theor. Chem. Acc.* **2016**, *135*, 75–84.

[23] G. La Penna, V. Minicozzi, S. Morante, G. C. Rossi, F. Stellato, *J. Chem. Phys.* **2015**, *143*, 124508–124515.

[24] W. L. Jorgensen, J. Chandrasekhar, J. D. Madura, R. W. Impey, M. J. Klein, *J. Chem. Phys.* **1983**, *79*, 926–935.

[25] J. Aaqvist, *J. Phys. Chem.* **1990**, *94*, 8021–8024.

[26] W. D. Cornell, P. Cieplak, C. I. Bayly, I. R. Gould, K. M. J. Merz, D. M. Ferguson, D. C. Spellmeyer, T. Fox, J. W. Caldwell, P. A. Kollman, *J. Am. Chem. Soc.* **1995**, *117*, 5179–5197.

[27] P. Raiteri, A. Laio, F. L. Gervasio, C. Micheletti, M. Parrinello, *J. Phys. Chem. B* **2006**, *110*, 3533–3539.

[28] P. Hošek, D. Toulcová, A. Bortolato, V. Spiwok, *J. Phys. Chem. B* **2016**, *120*, 2209–2215.

[29] J. C. Phillips, R. Braun, W. Wang, J. Gumbart, E. Tajkhorshid, E. Villa, C. Chipot, R. D. Skeel, L. Kalé, K. Schulten, *J. Comput. Chem.* **2005**, *26*, 1781–1802, http://www.ks.uiuc.edu/Research/namd.

[30] W. Humphrey, A. Dalke, K. Schulten, *J. Molec. Graphics* **1996**, *14*, 33–38, http://www.ks.uiuc.edu/Research/vmd.

[31] J.-P. Ryckaert, G. Ciccotti, H. J. C. Berendsen, *J. Comput. Phys.* **1977**, *23*, 327–341.

[32] U. Essmann, L. Perera, M. L. Berkowitz, T. Darden, H. Lee, L. G. Pedersen, *J. Chem. Phys.* **1995**, *103*, 8577–8593.

[33] H. J. C. Berendsen, J. P. M. Postma, W. F. Van Gunsteren, A. Di Nola, J. R. Haak, *J. Chem. Phys.* **1984**, *81*, 3684–3690.

[34] S. E. Feller, Y. Zhang, R. W. Pastor, B. R. Brooks, *J. Chem. Phys.* **1995**, *103*, 4613–4621.

[35] G. La Penna, S. Morante, A. Perico, G. C. Rossi, *J. Chem. Phys.* **2004**, *121*, 10725–10741.

[36] M. Elstner, D. Porezag, G. Jungnickel, J. Elsner, M. Haugk, T. Frauenheim, S. Suhai, G. Seifert, *Phys. Rev. B* **1998**, *58*, 7260–7268.

[37] B. Aradi, B. Hourahine, T. Frauenheim, *J. Phys. Chem. A* **2007**, *111*, 5678–5684.

[38] M. Bruschi, L. Bertini, V. Bonaci-Koutecký, De L. Gioia, R. Mitri, G. Zampella, P. Fantucci, *J. Phys. Chem. B* **2012**, *116*, 6250–6260.

[39] P. Giannozzi, S. Baroni, N. Bonini, M. Calandra, R. Car, C. Cavazzoni, D. Ceresoli, G. L. Chiarotti, M. Cococcioni, I. Dabo, A. Dal Corso, S. de Gironcoli, S. Fabris, G. Fratesi, R. Gebauer, U. Gerstmann, C. Gougoussis, A. Kokalj, M. Lazzeri, L. Martin-Samos, N. Marzari, F. Mauri, R. Mazzarello, S. Paolini, A. Pasquarello, L. Paulatto, C. Sbraccia, S. Scandolo, G. Sclauzero, A. P. Seitsonen, A. Smogunov, P. Umari, R. M. Wentzcovitch, *J. Phys. Condens. Matter* **2009**, *21*, 395502, http://www.quantum-espresso.org.

[40] D. Vanderbilt, *Phys. Rev. B* **1990**, *41*, 7892–7895.

[41] J. P. Perdew, K. Burke, M. Ernzerhof, *Phys. Rev. Lett.* **1996**, *77*, 3865–3868.

[42] Gaussian 09, Revision C.01, M. J. Frisch, M. J. Frisch, G. W. Trucks, H. B. Schlegel, G. E. Scuseria, M. A. Robb, J. R. Cheeseman, G. Scalmani, V. Barone, B. Mennucci, G. A. Petersson, H. Nakatsuji, M. Caricato, X. Li, H. P. Hratchian, A. F. Izmaylov, J. Bloino, G. Zheng, J. L. Sonnenberg, M. Hada, M. Ehara, K. Toyota, R. Fukuda, J. Hasegawa, M. Ishida, T. Nakajima, Y. Honda, O. Kitao, H. Nakai, T. Vreven, J. A. Montgomery, Jr., J. E. Peralta, F. Ogliaro, M. Bearpark, J. J. Heyd, E. Brothers, K. N. Kudin, V. N. Staroverov, R. Kobayashi, J. Normand, K. Raghavachari, A. Rendell, J. C. Burant, S. S. Iyengar, J. Tomasi, M. Cossi, N. Rega, N. J. Millam, M. Klene, J. E Knox, J. B. Cross, V. Bakken, C. Adamo, J. Jaramillo, R. Gomperts, R. E. Stratmann, O. Yazyev, A. J. Austin, R. Cammi, C. Pomelli, J. W. Ochterski, R. L. Martin, K. Morokuma, V. G. Zakrzewski, G. A. Voth, P. Salvador, J. J. Dannenberg, S. Dapprich, A. D. Daniels, Ö Farkas, J. B. Foresman, J. V. Ortiz, J. Cioslowski, D. J. Fox, Gaussian Inc., Wallingford CT, **2010**.

[43] Y. Zhao, D. G. Truhlar, *Theor. Chem. Acc.* **2008**, *120*, 215–241.

[44] A. V. Marenich, C. J. Cramer, D. G. Truhlar, *J. Phys. Chem. B* **2009**, *113*, 6378–6396.

[45] A. E. Reed, R. B. Weinstock, F. Weinhold, *J. Chem. Phys.* **1985**, *83*, 735–746.

[46] F. Eisenhaber, P. Lijnzaad, P. Argos, C. Sander, M. Scharf, *J. Comput. Chem.* **1995**, *16*, 273–284.

[47] T. Ooi, M. Oobatake, G. Némethy, H. A. Scheraga, *Proc. Natl. Acad. Sci. USA* **1987**, *84*, 3086–3090.

[48] W. Kabsch, *Acta Crystallogr. Sect. A* **1976**, *32*, 922–923.

◤◤ These are not the final page numbers!

Out of disorder: Transition metal ions often interact with disordered proteins. For example, the interaction of a single Cu ion with amyloid-β (Aβ) peptide and triplet O_2 is fundamental to producing reactive oxygen species in neurodegeneration. Hence, modelling of the Cu-Aβ-O_2 system was performed with the aim of dissecting the structural features that characterise dangerous Cu-based catalysts in neurodegeneration. This study showed that the production of superoxide is a process with low-energy intermediate species, once a small population of high-energy Cu^I-Aβ complex is formed (see figure).
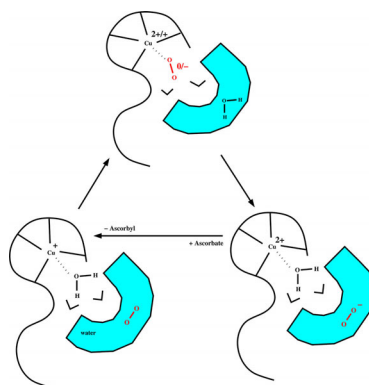
■ Disordered Proteins

G. La Penna,* M. S. Li

■■ – ■■

Towards High-Throughput Modelling of Copper Reactivity Induced by Structural Disorder in Amyloid Peptides